# System Level Performance Assessment of Large-Scale Cell-Free Massive MIMO Orientations with Cooperative Beamforming

**Panagiotis Gkonis[1], Spyros Lavdas[2,3], George Vardoulias[3], Panagiotis Trakadas[4], Lambros Sarakis[1] and Konstantinos Papadopoulos[1]**

[1]Department of Digital Industry Technologies, National and Kapodistrian University of Athens, Dirfies Messapies, Greece.
E-mails: {pgkonis, lsarakis, konspap}@dind.uoa.gr
[2]Department of Computer Science, Neapolis University, Paphos, Cyprus. E-mail: s.lavdas@nup.ac.cy
[3]Department of Information Technology, American College of Greece, Ag. Paraskeui, Greece. E-mails: {slavdas,gvardoulias}@acg.edu
[4]Department of Port Management and Shipping, National and Kapodistrian University of Athens, Dirfies Messapies, Greece.
E-mail: ptrakadas@uoa.gr

Corresponding author: Panagiotis Gkonis (e-mail: pgkonis@dind.uoa.gr).

**ABSTRACT** The goal of the study presented in this paper is to evaluate the performance of a proposed adaptive beamforming approach in cell-free massive multiple input multiple output (CF-mMIMO) orientations. To this end, mobile stations (MSs) can be served by multiple access points (APs) simultaneously. In the same context, the performance of a dynamic physical resource block (PRB) allocation approach is evaluated as well, where the set of assigned PRBs per active MS is constantly updated according to their signal strength and the amount of interference that cause to the rest of the co-channel MSs. Performance evaluation takes place in a two-tier wireless orientation, employing a system-level simulator designed for parallel Monte Carlo simulations. According to the presented results, a significant gain in energy efficiency (EE) can be achieved for medium data rate services when comparing the cell-free (CF) resource allocation approach to single AP links (non-CF). This is made feasible via cooperative beamforming, where on one hand, the radiation figures of the APs that serve a particular MS are jointly updated to ensure quality of service (QoS), and on the other hand, the effects of these updates on the other MSs are evaluated as well. Although EE for high data rate services decreases compared to the non-CF scenario, the proposed dynamic PRB allocation strategy significantly lowers the number of active radiating elements required to meet minimum QoS standards, thereby reducing both hardware and computational demands.

**INDEX TERMS** 5G, cell-free massive MIMO, millimeter-wave transmission, adaptive beamforming

## I. INTRODUCTION

The full deployment of fifth-generation (5G) networks is expected to support advanced services and applications on a large-scale, such as enhanced mobile broadband (eMBB) [1], ultra reliable low-latency communications (URLLC) [2] as well as massive machine type communications (mMTC) [3]. This is made feasible via the coexistence of various novel technologies both in the physical and network layer, such as millimeter wave (mmWave) transmission [4], massive multiple input multiple output (mMIMO) configurations [5] as well as non-orthogonal multiple access (NOMA) [6]. In the case of the mmWave transmission, the corresponding spectrum lies in the 30 GHz to 300 GHz range (with corresponding wavelengths from 10 mm to 1 mm). This spectrum area is of particular interest since it offers an order of magnitude more spectrum than lower bands. In addition, larger bandwidth channels are now possible (i.e., of 2 GHz, 4 GHz, 10 GHz or even 100 GHz). In the case of mMIMO, each antenna array configuration typically consists of hundreds or even thousands of radiating antenna elements. Therefore, there are more degrees of freedom in the design of adaptive beamforming techniques in densely deployed networks. Finally, in NOMA schemes multiple end users can utilize non-orthogonal resources concurrently by achieving a high spectral efficiency while allowing some degree of multiple access interference at the receivers.

As the demand for even higher data rates and the support of advanced services and applications is constantly increasing, the discussions on next generation networks are already underway. In this context, sixth-generation (6G) networks are expected to integrate a vast number of heterogeneous technologies and support dynamic network reconfiguration. In 6G communication systems, the use of higher frequency bands (mmWave, THz) and massive antenna arrays will enable high-accuracy and high-resolution sensing, paving the way towards integrated sensing and communication (ISAC) technologies [7], [8], [9]. To this end, the entire network can act as a sensor obtaining various metrics, such as range, velocity, and angle information from the radio signals. Hence, accuracy localization, gesture capturing and activity recognition, passive object detection and tracking, as well as imaging and environment reconstruction can be supported. Indicative use cases include holographic communication-based services, unmanned mobility, etc. [10], [11]. In this new era of 6G networks, it is expected that the traditional base station (BS) – mobile station (MS) link model will be replaced by a large number of low power access points (APs) over small geographical areas [12] (ultra dense networks - UDNs). In the same context, relay nodes (RNs) that can amplify and retransmit the received signal will also be an indispensable part of 6G networks, especially for cell-edge spatial coverage [13].

The concept of cell-free massive MIMO (CF-mMIMO) orientations has recently emerged as a new approach that can provide on-demand coverage in large geographical areas [14], [15]. In this context, mMIMO configurations are deployed per AP to support a multitude of active MSs via highly directional beams (an MS can be served by multiple APs). CF-mMIMO systems comprise of many distributed, low-cost, and low power access point antennas, connected to a network controller. The complexity and signalling at each AP can be finite even when the number of MSs approaches infinity [16]. This is made feasible via appropriate clustering and power control algorithms that enable scalability. CF-mMIMO configurations are expected to enhance the support of highly demanding mobility patterns, as traffic load can be balanced among the APs and the handover signalling burden can be reduced. Moreover, in realistic wireless orientations signal quality and cell-edge coverage can be improved, due to the multitude of available channels from the various APs. In the same context, appropriate machine learning (ML) approaches can be also applied that can reduce the computational complexity of mMIMO deployments (e.g., optimum beamforming configuration per AP, transmission vector matrix formulation, power allocation, user grouping when mMIMO technology is combined with NOMA) [17], [18].

Despite growing scientific interest in CF-mMIMO systems in recent years, as highlighted by key studies outlined in the next subsection, conducting a comprehensive performance evaluation is crucial to uncover any potential limitations and deployment challenges. Therefore, the goal of this work is to evaluate the performance of CF-mMIMO orientations with respect to conventional centralized mMIMO approaches (non-CF) under the prism of a proposed dynamic physical resource block (PRB) allocation approach and cooperative adaptive beamforming. To this end, various key performance indicators (KPIs) have been considered, such as energy and spectral efficiency (EE, SE), blocking probability (BP), and the number of radiating elements (REs) in the topology.

## A. INDICATIVE RELATED WORKS

Over the last decade, various research activities have focused on the performance evaluation of CF-mMIMO orientations. In [19], the main challenges, solutions, and opportunities for user-centric CF-mMIMO networks are presented. The work in [20] considers practical measurements of CF-mMIMO systems. In this context, three different co-located and widely distributed radio unit (RU) configurations have been analyzed in terms of time-variant delay-spread, Doppler spread, path-loss, and the correlation of the local scattering function over space. Results indicate that various performance metrics can be improved, such as signal-to-interference-plus-noise ratio (SINR). Moreover, as the authors point out, CF systems are less susceptible to channel aging than distributed or conventional mMIMO systems. The work in [21] deals with more flexible architectures that are based on wireless fronthaul operating at a higher band compared to the access links. Results indicate that these architectures can achieve comparable data rates to those obtained with optical fiber-based fronthaul. Hence, installation complexity and related costs can be reduced.

In [22], the performance of CF-mMIMO systems is examined in an industrial indoor scenario to assist inspection robots. To this end, AP selection, power control and scalability issues are examined. In [23], the authors investigate isolated and cumulative failures on the hardware of CF-mMIMO networks, concluding that system performance degradation can be significantly increased as the MS density increases. Therefore, appropriate protection schemes are required that can mitigate failure effects. In [24], the performance of asynchronous CF-mMIMO systems with rate-splitting has been evaluated. In this context, closed-form expressions have been derived in the presence of channel estimation errors. Results indicate that asynchronous reception can have a severe impact on the pilot orthogonality and coherent data transmission. Hence, suitable precoding schemes have been designed to maximize the SE. In [25], a new CF architecture is proposed for virtualized cloud radio access network (V-CRANs). In this context, end to end power consumption is minimized, by optimally selecting APs and distributed units (DUs) per active MS.

**IEEE** *Access*
Multidisciplinary : Rapid Review : Open Access Journal

TABLE I
LIST OF ACRONYMS

| | | | |
|---|---|---|---|
| 5G/6G | Fifth/Six Generation | mmWave | Millimeter Wave |
| 3GPP | Third Generation Partnership Project | MMSE | Minimum Mean-Squared Error |
| AP | Access Point | mMTC | Massive Machine-Type Communications |
| BP | Blocking Probability | MO | Modulation Order |
| BS | Base Station | MoM | Method of Moments |
| BSA | BS Allocation | MRC | Maximal Ratio Combining |
| CDF | Cumulative Distribution Function | MS | Mobile Station |
| CCI | Co-Channe Interference | NLOS | Non-Line of Sight |
| CF | Cell Free | NOMA | Non-Orthogonal Multiple Access |
| CFA | CFA Cell Free Allocation | PRB | Physical Resource Block |
| CG | CG Channel Gain | QoS | Quality of Service |
| CSI | CSI Channel State Information | RE | Radiating Element |
| CPU | Central Processing Unit | RF | Radio Frequency |
| DU | Distributed Unit | RHCP | Right Hand Circular Polarization |
| EE | Energy Efficiency | RN | Relay Node |
| eMBB | Enhanced Mobile Broadband | RU | Radio Unit |
| HBF | Hybrid Beamforming | SE | Spectral Efficiency |
| IoT | Internet of Things | SINR | Signal to Interference plus Noise Ratio |
| ISAC | Integrated Sensing And Communication | SJR | Signal to Jamming Ratio |
| KPI | Key Performance Indicator | TS | Traffic Scenario |
| LHCP | Left Hand Circular Polarization (LHCP) | UDN | Ultra Dense Network |
| MC | Monte Carlo | URLLC | Ultra Reliable Low Latency Communications |
| ML | Machine Learning | V-CRAN | Virtualized Cloud Radio Access Network |
| mMIMO | Massive Multiple Input Multiple Output | XPR | Cross Polarization Power Ratio |

In [26], the resource allocation for a CF-mMIMO enabled URLLC downlink system is studied, and closed-form solutions are derived for the lower bound data rate based on imperfect channel state information (CSI). The derived non-convex problem is transformed to a discrete set of subproblems, that are iteratively solved via a proposed low complexity approach. In [27], the concept of hybrid beamforming (HBF) is considered, where fewer radio frequency (RF) chains are employed compared to the number of active antenna elements in the topology. Hence, signalling burden and computational complexity of mMIMO configurations can be reduced. To achieve that, the subset of antennas that are associated with a specific RF chain can adjust their phases in an analogue mode. Thus, when considering multiple APs equipped with HBF, for each possible MS, a set of candidate RF chains that have the highest received signal power is defined, without considering the specific APs these RF chains are associated with.

According to the presented results, the proposed approach can significantly improve SE and reduce the complexity of centralized beamforming. In [28], data-assisted channel estimation has been considered. In this context, the analytical achievable uplink SE for minimum mean-squared error (MMSE) combining has been derived. In [29], a multi-CPU CF-mMIMO orientation is considered, where the effect of quantization noise caused by capacity-limited backhaul links is investigated. Also, a new MMSE beamformer and clustering methods have been developed, where the joint resource optimization problem is solved.

In [30] the authors have derived closed-form expressions for the lower-bound achievable rate and SE under maximum ratio combining (MRC) and imperfect CSI, considering a CF-mMIMO internet of things (IoT) network. Moreover, a low-complexity power control approach is presented, based on local CSI. As the authors point out, the addition of more transmit antennas can enhance the achievable rate but may degrade the achievable SE due to the increased pilot overhead.

In [31], a two-layer large scale fading precoding method is proposed in a downlink CF-mMIMO system. In this context, in the first layer the distributed APs are responsible for designing distributed precoding and power control coefficients for the MSs. In the second layer, the CPUs perform zero forcing processing to mitigate the interference caused by pilot contamination. Finally, the work in [32] considers hardware impairments in an uplink CF-mMIMO system. In this context, closed-form expressions of SE have been derived, which prove that the effect of hardware impairments can be mitigated in the case of MSs with multiple antennas.

### B. CONTRIBUTIONS

In all the aforementioned studies, either limited network topologies have been considered (i.e. single-cell scenarios) or a limited number of active MSs. In this work, a two-tier topology (19 active cells) is taken into consideration, with three APs per cell. An MS can be served either by one AP that is selected according to total losses minimization (centralized provision of service, non-CF) or in a CF mode. In the same context, a dynamic PRB allocation scheme is also considered, that is based on a continuous resource reconfiguration according to channel conditions and overall interference. Therefore, the main contributions of our work can be summarized as follows:

- Performance evaluation of CF-mMIMO orientations takes place in large-scale wireless environments. For this purpose, a system level simulator has been developed that can execute independent Monte Carlo (MC) simulations in parallel. In this context, various system orientations are generated (each one corresponding to a different MS distribution and channel generation of the corresponding PRBs) where dynamic PRB assignment and power allocation procedures take place. At each MC snapshot various KPIs are extracted, such as EE, SE, BP and number of REs.
- A PRB allocation approach is presented and evaluated, that can further improve performance metrics. This approach is based on a dynamic update of the allocated PRBs, according to channel conditions and interference levels. As it will also be explained in Section IV, PRB assignment is based on the SINR per MS and PRB as well as on the amount of interference that this MS causes to the rest of co-channel MSs.
- Transmission in mmWave frequency band has been also considered (i.e., 28 GHz), incorporating recent 3GPP channel modelling guidelines [33].

To the best of the authors' knowledge, this is the first scientific attempt where realistic radiation patterns are used for the performance evaluation of CF-mMIMO orientations. The rest of this paper is organized as follows: In Section II, the 5G mmWave multicellular mMIMO orientation is presented (channel modelling and transceiver procedures), while in Section III the antenna design aspects per AP are highlighted. In Section IV, the proposed resource allocation and adaptive beamforming approaches are analyzed, for both considered orientations (centralized provision of service as well as CF transmission mode). Results are presented in Section V, where the previously mentioned KPIs have been considered. Finally, concluding remarks and proposals for future work are provided in Section VI.

The following notation is used in the paper. An italic variable $a$ or $A$ denotes a scalar, whereas boldface lowercase and uppercase variables $\mathbf{a}$ and $\mathbf{A}$ denote vectors and matrices, respectively (the $(i,j)$ element of $\mathbf{A}$ is denoted as $A(i,j)$). Moreover, $\|\mathbf{a}\|_F$ stands for the Frobenius norm of vector $\mathbf{a}$. A calligraphic variable $\mathcal{A}$ denotes a set of $|\mathcal{A}|$ elements ($\overline{\mathcal{A}}$ is the complementary set), while $\mathbf{A}^H$ denotes the conjugate transpose of matrix $\mathbf{A}$.

## II. 5G MILLIMETER WAVE MASSIVE MIMO ORIENTATION

We consider the downlink of a 5G mMIMO multicellular orientation with $B$ BSs, as shown in Fig. 1. To this end, there are three APs per BS that can provide sufficient signal coverage. The total available bandwidth is denoted as $W$ and is divided to a discrete number of PRBs [34]. MSs enter the network sequentially following a predefined spatial distribution. In CF-mMIMO mode, PRBs may be allocated from adjacent APs as well. Throughout the rest of this paper, the term adjacent APs will indicate the set of APs that belong to geographically adjacent BSs (i.e., first tier BSs with respect to the specific AP) and their radiation patterns might have an impact on co-channel interference (CCI). It should be emphasized at this point that since two operational modes have been considered (non-CF and CF), the BS concept with three APs in its area of service is adopted for the non-CF case. Each MS that enters the network is assumed to request a specific type of service that is translated to an equivalent number of assigned PRBs, as it will be later described in Section IV.

In each AP there are 441 REs, that are deployed in an orthogonal configuration (21 arrays per dimension) able to formulate a multitude of radiation diagrams that can be steered across the AP's serving area, as it will be described in in the following section. In the non-CF mMIMO operational mode, blocking occurs if there are no available PRBs in the serving BS of the candidate MS. On the contrary, in the CF-mMIMO case, this happens either if there are no available PRBs in the adjacent APs, or their potential allocation would result in excessive downlink transmission power.

In the following two subsections, channel modelling issues along with transceiver procedures are described. In particular, in Subsection A the main 3GPP guidelines for mmWave transmission are summarized, while in Subsection B signal transmission and reception over all APs are highlighted.

## A. CHANNEL MODELLING

Considering a non-line of sight (NLOS) environment, the channel impulse response for an arbitrary pair of transmitting-receiving antennas (denoted as $q$ and $u$, respectively, $1 \leq q \leq N_t$, $1 \leq u \leq N_r$) is given by [33]:

$$H_{u,q}^{\text{NLOS}}(\tau,t) = \sum_{n=1}^{2} \sum_{i=1}^{3} \sum_{m \in \mathcal{R}_i} H_{u,q,n,m}^{\text{NLOS}}(t)\delta(t-\tau_{n,i}) + \sum_{n=3}^{N} H_{u,q,n}^{\text{NLOS}}(t)\delta(t-\tau_n)$$
(1)

where $\tau_{n,i}$, $\tau_n$ represent the delay of the $i^{\text{th}}$ subcluster of the $n^{\text{th}}$ cluster and the delay of the $n^{\text{th}}$ cluster, respectively, and $\delta$ stands for the Kronecker delta. It is important to note that for the first two dominant clusters three additional sub-clusters are defined. The subpaths per sub-cluster are stored in the set $\mathcal{R}_i$. Moreover, $H_{u,q,n,m}^{\text{NLOS}}$ and $H_{u,q,n}^{\text{NLOS}}$ are given by:

$$H_{u,q,n,m}^{\text{NLOS}} = \sqrt{\frac{P_n}{M}} \mathbf{F}_{rx,n,m}^{\text{T}} \boldsymbol{\Theta}_{n,m} \mathbf{F}_{tx,n,m} e^{\frac{j2\pi(\hat{r}_{rx,n,m}^{\text{T}} \cdot \bar{d}_{rx,u})}{\lambda_o}} e^{\frac{j2\pi(\hat{r}_{tx,n,m}^{\text{T}} \cdot \bar{d}_{tx,q})}{\lambda_o}}$$
(2)

$$H_{u,q,n}^{\text{NLOS}} = \sum_{m=1}^{M} H_{u,q,n,m}^{\text{NLOS}}$$
(3)

where:

$$\mathbf{F}_{rx,n,m} = \begin{bmatrix} F_{rx,u,\theta}(\theta_{n,m,ZOA}, \phi_{n,m,AOA}) \\ F_{rx,u,\phi}(\theta_{n,m,ZOA}, \phi_{n,m,AOA}) \end{bmatrix}$$
(4)

$$\mathbf{F}_{tx,n,m} = \begin{bmatrix} F_{tx,q,\theta}(\theta_{n,m,ZOD}, \phi_{n,m,AOD}) \\ F_{tx,q,\phi}(\theta_{n,m,ZOD}, \phi_{n,m,AOD}) \end{bmatrix}$$
(5)

$$\boldsymbol{\Theta}_{n,m} = \begin{bmatrix} \exp(j\Phi_{n,m}^{\theta\theta}) & \sqrt{\kappa_{n,m}^{-1}} \exp(j\Phi_{n,m}^{\theta\phi}) \\ \sqrt{\kappa_{n,m}^{-1}} \exp(j\Phi_{n,m}^{\phi\theta}) & \exp(j\Phi_{n,m}^{\phi\phi}) \end{bmatrix}$$
(6)

In the above set of equations, $\theta_{n,m,ZoD}$ and $\theta_{n,m,ZoA}$ represent the angles of departure (AoD) and arrival (AoA), respectively, in the vertical plane for the $m^{\text{th}}$ subpath ($1 \leq m \leq M$) of the $n^{\text{th}}$ cluster ($1 \leq n \leq N$). The corresponding parameters for the horizontal plane are $\phi_{n,m,AoD}$ and $\phi_{n,m,AoA}$, respectively. Moreover, $P_n$ is the power of the $n^{\text{th}}$ cluster, the set $\{\Phi_{n,m}^{\theta\theta}, \Phi_{n,m}^{\theta\phi}, \Phi_{n,m}^{\phi\theta}, \Phi_{n,m}^{\phi\phi}\}$ corresponds to initial phases uniformly distributed in $(-\pi,\pi)$ while $\kappa_{n,m}$ parameter is the generated cross polarization power ratio (XPR) for each ray $m$ of cluster $n$. In addition, $\hat{r}_{rx,n,m}$ is the spherical unit vector with azimuth arrival angle $\phi_{n,m,AOA}$ and elevation arrival angle $\theta_{n,m,ZOA}$, while $\hat{r}_{tx,n,m}$ is the spherical unit vector with azimuth departure angle $\phi_{n,m,AOD}$ and elevation departure angle $\theta_{n,m,ZOD}$.
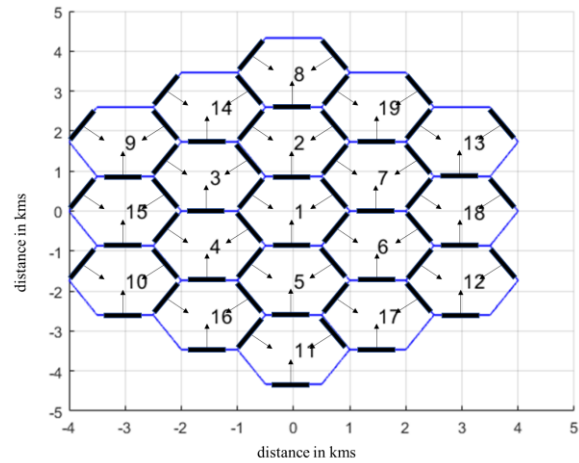
Moreover, $\mathbf{F}_{tx}$/$\mathbf{F}_{rx}$ represent the field pattern of transmitting/receiving antenna element $q/u$, respectively, $\bar{d}_{rx,u}$ is the location vector of receive antenna element $u$ and $\bar{d}_{tx,q}$ is the location vector of transmit antenna element $q$. Finally, $\lambda_o$ is the carrier wavelength. Note that in cases of LOS environments $\boldsymbol{\Theta}_{n,m}$ is a diagonal matrix with elements +1 and -1 appearing on the diagonal.

## B. TRANSCEIVER PROCEDURES

The $N_t \times 1$ transmitted signal in the CF-mMIMO orientation can be expressed as:

$$\mathbf{x}_k(t) = \sum_{s \in \mathcal{U}_k} \sqrt{p_{k,\text{T}(k,s),s}} \mathbf{t}_{k,\text{T}(k,s),s} X_{k,s} e^{j2\pi f_s t}, 0 < t < T_s \quad (7)$$

where the set $\mathcal{U}_k$ indicates the assigned PRBs to the $k^{\text{th}}$ MS ($1 \leq k \leq K$). Moreover, $\text{T}(k,s)$ is the corresponding entry of 2D matrix $\mathbf{T}$ that indicates the serving AP of the $k^{\text{th}}$ MS with respect to the $s^{\text{th}}$ PRB, $p_{k,\text{T}(k,s),s}$ is the corresponding downlink transmission power and $\mathbf{t}_{k,\text{T}(k,s),s}$ is the $N_t \times 1$ transmission weight vector. It should be emphasized at this point that diversity combining transmission mode is assumed. Moreover, $X_{k,s}$ is the transmission symbol over the $s^{\text{th}}$ PRB selected from a predefined signal constellation (i.e., QPSK, 16QAM, 64QAM), $f_s$ is the frequency of the $s^{\text{th}}$ PRB and $T_s$ is the symbol duration.

In reception mode, the corresponding $N_r \times 1$ signal after matched filtering over the $s^{\text{th}}$ PRB can be expressed as:

$$\mathbf{Y}_{k,s} = \left( \sqrt{\frac{p_{k,\text{T}(k,s),s}}{TL_{k,\text{T}(k',s)}}} \right) \mathbf{r}_{k,\text{T}(k,s),s} \mathbf{H}_{k,\text{T}(k,s),s} \mathbf{t}_{k,\text{T}(k,s),s} X_{k,s} +$$

$$\sum_{k' \neq k, s \in \mathcal{U}_{k'}}^{K} \left( \sqrt{\frac{p_{k',\text{T}(k',s),s}}{TL_{k,\text{T}(k',s)}}} \right) \mathbf{r}_{k,\text{T}(k,s),s} \mathbf{H}_{k,\text{T}(k',s),s} \mathbf{t}_{k',\text{T}(k',s),s} X_{k',s} + \mathbf{r}_{k,\text{T}(k,s),s} \mathbf{n}_{k,s}$$
(8)

The first term is the desired MS signal, while the second/third term denote CCI and noise, respectively. In the same context, $\mathbf{H}_{k,\mathrm{T}(k,s),s}$ is the $N_r \times N_t$ channel matrix of the $k^{\mathrm{th}}$ MS with respect to the $s^{\mathrm{th}}$ PRB and $\mathbf{r}_{k,\mathrm{T}(k,s),s}$ is the $1 \times N_r$ MRC multiplying vector. Finally, $TL_{k,\mathrm{T}(k,s)}$ represents the total losses (including shadowing and attenuation due to radiation patterns). The SINR per MS and PRB in CFA allocation mode averaged over a frame duration can be expressed as (assuming that $\mathrm{E}(X_{k,s} X_{k',s}) = \delta_{k,k'}$, where $\mathrm{E}(x)$ is the mean value of $x$):

$$SINR_{k,s} = \frac{\dfrac{p_{k,\mathrm{T}(k,s),s}}{TL_{k,\mathrm{T}(k,s),}} \left| \mathbf{r}_{k,s} \mathbf{H}_{k,\mathrm{T}(k,s),s} \mathbf{t}_{k,\mathrm{T}(k,s),s} \right|^2}{\displaystyle\sum_{k' \neq k, s \in \mathcal{U}_{k,}} \dfrac{p_{k',\mathrm{T}(k',s),s}}{TL_{k,\mathrm{T}(k',s)}} \left| \mathbf{r}_{k,s} \mathbf{H}_{k,\mathrm{T}(k',s),s} \mathbf{t}_{k',\mathrm{T}(k'),s} \right|^2 + \mathbf{r}_{k,\mathrm{T}(k,s),s}^{\mathrm{H}} \mathbf{r}_{k,\mathrm{T}(k,s),s} I_o}$$

(9)

where $I_o$ is the thermal noise level.

From (9), it follows that the ratio of the desired signal power of a particular MS to the total amount of interference that causes to the of rest co-channel MSs (also referred as jamming) can be expressed as:

$$SJR_{k,s} = \frac{\mathbf{t}_{k,\mathrm{T}(k,s),s}^{\mathrm{H}} \left( \mathbf{H}_{k,\mathrm{T}(k,s),s}^{\mathrm{H}} \mathbf{H}_{k,\mathrm{T}(k,s),s} \right) \mathbf{t}_{k,\mathrm{T}(k,s),s}^{\mathrm{H}}}{\mathbf{t}_{k,\mathrm{T}(k,s),s}^{\mathrm{H}} \left( \displaystyle\sum_{k' \neq k, s \in \mathcal{U}_{k,}} \mathbf{H}_{k',\mathrm{T}(k,s),s}^{\mathrm{H}} \mathbf{H}_{k',\mathrm{T}(k,s),s} \left( \dfrac{TL_{k,\mathrm{T}(k,s)}}{TL_{k',\mathrm{T}(k,s)}} \right) + I_o TL_{k,\mathrm{T}(k,s)} \right) \mathbf{t}_{k,\mathrm{T}(k,s),s}}$$

(10)

Assuming that each MS requests $R_k$ Mbps from the serving APs, then SE and EE can be defined as follows:

$$SE = \frac{\displaystyle\sum_{k=1}^{K} R_k}{W} \qquad (11)$$

$$EE = \frac{\displaystyle\sum_{k=1}^{K} R_k}{\displaystyle\sum_{k=1}^{K} \sum_{s \in \mathcal{U}_k} p_{k,\mathrm{T}(k,s),s}} \qquad (12)$$

## III. ANTENNA DESIGN

The current work employs a cost-effective antenna array configuration to minimize hardware complexity. Specifically, the suggested mmWave antenna setup features a 21×21 array of rounded crossed bowtie REs, as illustrated in Fig. 2. To achieve a unidirectional radiation pattern with minimal energy wastage through the back lobe, two ground planes are positioned beneath each RE at distances of $\lambda_o/4$ and $\lambda_o/2$, respectively, with reference to each rounded bowtie antenna [35]. Notably, the crossed rounded bowtie antennas, serving as exciters of the reflector, are rotated at ±45° to enhance the formulation of an adaptive dual-polarized radiation pattern which is crucial for cellular network communications [36].

In particular, the former rotation of the exciters, coming with a phase difference of 90°, facilitates the creation of circular polarization, achieving high cross polarization power ratio (XPR) values more than 20 dB for the desired spatial coverage. This occurs because right-hand circular polarization (RHCP), which is the current main polarization, and left-hand circular polarization (LHCP) are naturally well-isolated. High XPR values, in concert with circular polarization, reduce not only the sensitivity to the orientation of the receiving antenna—which is beneficial in mobile communications where antenna orientations can significantly vary—but interference levels as well, and at the same time improve signal integrity. To this end, such an antenna scheme leads to improved overall system performance.

It is essential to mention at this point that the detailed electromagnetic characteristics of this array configuration are thoroughly covered in our recent publications [37], [38] (radiation diagrams and technical details about the REs have been included as well). The analysis employs the method of moments (MoM) [39] in a 3D computational model [40], accounting for the deleterious effects of mutual coupling among REs. The adoption of different phases for each RE, coupled with activating either the entire array or a subarray, facilitates the deployment of efficient beamforming techniques. This enhances the manipulation of the radiation pattern, allowing changes in both desired directions (azimuth or elevation level) and gain [39]. Fig. 2 illustrates an example of the applied beamforming configurations, demonstrating 2 out of 51 different possible configurations, including square and rectangular arrays [38].

The choice of the right array configuration takes into consideration three key parameters: the number of activated REs, the desired quality of service (QoS), and the required spatial coverage. In this context, six representative scenarios showcasing the mutual dependence of these parameters are presented in Fig. 2. In particular, the left panel demonstrates three different radiation patterns in azimuth where all of them are derived from the same 3×3 square subarray. As it has already been mentioned, the appropriate applied phase difference among the REs leads to an efficient beamforming configuration, namely achieving a spatial coverage between +30° and -30°. In the same context, the right panel of Fig. 2 illustrates the same spatial coverage by employing a larger square subarray of 11×11 REs. However, the developed radiation patterns are not only significantly more directional but also offer greater spatial gain. As a result, this setup is ideally suited for cellular network applications that require high service standards.

Therefore, by adapting to various QoS levels, the algorithm can effectively choose the optimal subarray configuration in terms of power consumption, gain efficiency, and spatial coverage. Specifically, the underlying principle of the employed algorithm for activating the appropriate radiating subarray is to effectively provide the required services while minimizing energy consumption.
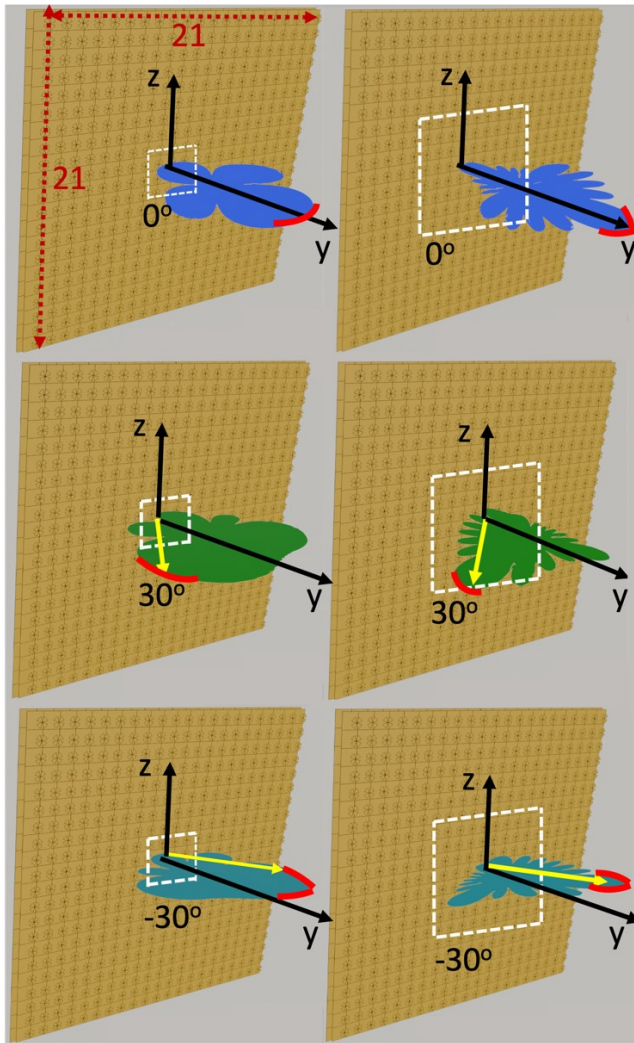
**FIGURE 2.** Two square subarray beamforming configurations: 3×3 (left) and 11×11 (right) with corresponding azimuth radiation patterns for 0°, 30°, and -30° spatial coverage (red outlines indicate positive gain in the left panel, doubling the values in gain in the right panel).

By dynamically adjusting the active subarrays based on real-time demand, the algorithm ensures optimal performance and energy efficiency, thereby enhancing the overall performance of the communication channel. It's important to highlight that changes in the configuration can be made using affordable pin diodes to activate the necessary REs. Additionally, integrating ML techniques could further enhance these configurations [38].

## IV. COOPERATIVE ADAPTIVE BEAMFORMING IN CELL-FREE MASSIVE MIMO ORIENTATIONS

### A. ALGORITHM DESCRIPTION

The proposed resource allocation approach in CF-mMIMO orientations is described in Algorithm I. At the first step, all active BSs are initialized with the same number of PRBs (i.e., the set $\mathcal{S}_b$ indicates the available PRBs in the $b^{th}$ BS, $1 \leq b \leq B$). In the same context, the REs per AP are initialized as well (i.e., the set $\mathcal{TE}_{b,l}$ indicates the

transmitting elements in the $l^{th}$ AP of the $b^{th}$ BS, $1 \leq l \leq 3$, while all potential beamforming configurations are stored in the set $\mathcal{BC}_{b,l}$).

There are two possible modes during PRB allocation: In the first case, which will be denoted as BS allocation (BSA), PRB assignment is based on the active PRBs of the specific BS. In the second case, denoted as CF allocation (CFA), all APs of the adjacent BSs participate in PRB allocation. In the same context, a dynamic PRB allocation approach is also examined, that is based on PRB switching according to channel conditions and overall interference levels. In this approach, for every new MS that tries to access the network, all PRBs of adjacent APs are considered as available, even the occupied ones.

The adjacent APs with respect to the $b^{th}$ BS are stored in the set $\mathcal{J}_b$. If channel gain (stored in matrix **CG**) is maximized for a particular PRB that has already been assigned to another MS, then PRB switching might take place: In this case, it is examined if in the new state, where the potential new MS is allocated with the PRB that maximizes its channel gain and the other MS is allocated with the next available PRB, the product of SINR and SJR is maximized. In all cases, the indexes of the sorted channel gains are stored in the set $\mathcal{U}_k$, which indicates the allocated PRBs to the $k^{th}$ MS, as previously mentioned.

As described in Algorithm I, the $k^{th}$ MS tries to enter the network in the serving area of the $b^{th}$ BS requesting $R_k$ Mbps with a specific modulation order ($MO_k$) per PRB. This request is translated into an equivalent number of PRBs with the help of function *define_PRBs*. In step 4, control flag $c_f$ indicates either the BSA ($c_f = 0$) or the CFA mode ($c_f = 1$). In both cases, the $P$ equivalent channel gains are sorted, and the results are stored in the set $\mathcal{U}_k$ (or $\mathcal{U}_{k,opt}$).

In Step 6, considering the dynamic PRB allocation approach ($d_f = 1$), if the selected PRB is already assigned to another MS (i.e., the $k'^{th}$ MS), then a temporal allocation is performed according to which this PRB is assigned to the new potential MS and the $k'^{th}$ MS is assigned with the next available PRB. In this new state, if the product of the updated SINR and SJR values for both MSs is increased compared to the previous state, then PRB allocation as previously described takes place. Otherwise, the new potential MS is assigned with another PRB that has already been calculated in Step 4. In both cases, beamforming and power assignment calculations take place (i.e., $\mathbf{x}(\lambda_m(\mathbf{A}))$) is the eigenvector corresponding to the maximum eigenvalue of matrix $\mathbf{A}$).

In the same context, it is essential to examine if power outage in at least one of the active MSs takes place. In this case, additional beamforming configurations are examined (i.e., the set $\mathcal{MS}_b$ denotes the active MSs in the $b^{th}$ BS). To this end, the term $\sum_{s \in \mathcal{U}_{k'}} p_{k',s} \leq p_m$ indicates total downlink transmission power from the $k'^{th}$ MS, which is upper limited by $p_m$.

ALGORITHM I

| |
|---|
| The Proposed Cooperative Adaptive Beamforming and Resource Allocation Approach in Cell-Free Massive MIMO orientations |

1: $\mathcal{S}_b \leftarrow \{1 : N_{PRB}\}$, *initialize* $\mathcal{TE}_{b,l}$, $1 \le l \le 3$

2: $k \leftarrow k+1$. The $k^{\text{th}}$ MS enters the network in the $b^{\text{th}}$ BS requesting $R_k$ Mbps with a specific modulation order ($MO_k$) per PRB

3: $P \leftarrow define\_PRBs(R_k, MO_k)$

4: **if** ($c_f = 0$) (BSA mode)

$\mathbf{CG}_{\mathcal{S}_b} \leftarrow \left\| \mathbf{H}_{k,\mathcal{S}_b}^{\text{H}} \right\|_F^2 / TL_{k,\mathcal{S}_b}$, $\left[ \sim, \mathcal{U}_k \right] \leftarrow sort(\mathbf{CG}_{\mathcal{S}_b}, P)$

**else** (CFA mode)

$\mathbf{CG}_{\mathcal{S}_{\mathcal{J}_b}} \leftarrow \left\| \mathbf{H}_{k,\mathcal{S}_{\mathcal{J}_b}}^{\text{H}} \right\|_F^2 / TL_{k,\mathcal{S}_{\mathcal{J}_b}}$

$\left[ \sim, \mathcal{U}_k \right] \leftarrow sort(\mathbf{CG}_{\mathcal{S}_{\mathcal{J}_b}}, P)$

**end if**

5: **if** ($d_f = 1$) (the proposed dynamic PRB approach)

$\mathbf{CG}_{\mathcal{S}_{\mathcal{J}_b} \cup \overline{\mathcal{S}_{\mathcal{J}_b}}} \leftarrow \left\| \mathbf{H}_{k,\mathcal{S}_{\mathcal{J}_b} \cup \overline{\mathcal{S}_{\mathcal{J}_b}}}^{\text{H}} \right\|_F^2 / TL_{k,\mathcal{S}_{\mathcal{J}_b} \cup \overline{\mathcal{S}_{\mathcal{J}_b}}}$

$\left[ \sim, \mathcal{U}_{k,opt} \right] \leftarrow sort(\mathbf{CG}_{\mathcal{S}_{\mathcal{J}_b} \cup \overline{\mathcal{S}_{\mathcal{J}_b}}}, P)$

**end if**

6: **for** $s \in \mathcal{U}_k$ (or $s_{opt} \in \mathcal{U}_{k,opt}$, if $d_f = 1$)

**if** $s_{opt} \notin \mathcal{S}_b$ (which means that $d_f = 1$ and the selected PRB is occupied by the $k^{\text{th}}$ MS)

$s_1 \leftarrow s_{opt}$, $s_2 \leftarrow \mathcal{U}_{k'}(P+1)$, $s_3 \leftarrow s$, $s_4 \leftarrow s_{opt}$

**if** $\begin{aligned} &SINR_{k,s_1} \cdot SJR_{k,s_1} \cdot SINR_{k',s_2} \cdot SJR_{k',s_2} > \\ &SINR_{k,s_3} \cdot SJR_{k,s_3} \cdot SINR_{k',s_4} \cdot SJR_{k',s_4} \end{aligned}$

$\mathcal{U}_k \leftarrow \mathcal{U}_k \cup s_{opt}$, $\mathcal{U}_{k'} \leftarrow \mathcal{U}_{k'} - s_{opt}$

**end if**

**end if**

$\mathbf{t}_{k,\text{T}(k,s),s} \leftarrow \mathbf{x}\left( \lambda_m \left( \mathbf{H}_{k,\text{T}(k,s),s}^{\text{H}} \mathbf{H}_{k,\text{T}(k,s),s} \right) \right)$, $p_{k,\text{T}(k,s)} \leftarrow \dfrac{SNR_{th} \cdot I_o \cdot TL_{k,\text{T}(k,s)}}{\left\| \mathbf{H}_{k,\text{T}(k,s)} \mathbf{t}_{k,\text{T}(k,s),s} \right\|_F^2}$

*update* $p_{k',\text{T}(k',s),s}$, $1 \le k' \le K$, $s \in \mathcal{U}_k$ or $s_{opt} \in \mathcal{U}_{k',opt}$

**end for**

7: **if** $\sum_{s \in \mathcal{U}_{k'}} p_{k',\text{T}(k',s),s} \le p_m$, $1 \le k' \le K$ **then** $rf \leftarrow 0$

**else**

**for every** $b \in \mathcal{J}_b$

**while** $\left\{ \left( |\mathcal{BC}_{b,l}| > 0 \right) \text{ and } (rf > 0) \right.$

$\mathcal{TE}_{b,l} \leftarrow \underset{\mathcal{Q}' \in \mathcal{BC}_{b,l}}{argmin} \left( |\mathcal{Q}'| \right)$, $\mathcal{BC}_{b,l} \leftarrow \mathcal{BC}_{b,l} - \mathcal{TE}_{b,l}$

*update* $\mathbf{H}_{k',\text{T}(k',s),s}, \mathbf{t}_{k',\text{T}(k',s),s}, p_{k',\text{T}(k',s),s}$ for every $k' \in \mathcal{MS}_b, s \in \mathcal{U}_k$.

**if** $\sum_{s \in \mathcal{U}_{k'}} p_{k',\text{T}(k',s),s} \ge p_m$ for an arbitrary $k' \in \mathcal{MS}_b$, then

$rf \leftarrow 1$, *restore* $\mathbf{H}_{k',\text{T}(k',s),s}, \mathbf{t}_{k',\text{T}(k',s),s}, p_{k',\text{T}(k',s),s}$ and $\mathcal{BC}_{b,l}$

**end if**

**end while**

**end for**

**end if**

8: **if** $rf = 0$, then

$\mathcal{S}_b \leftarrow \mathcal{S}_b - \mathcal{U}_k$, $\mathcal{MS}_b \leftarrow \mathcal{MS}_b \cup k$

Set $P_{t,b} \leftarrow \sum_{k' \in \mathcal{MS}_b, s \in \mathcal{U}_{k'}} p_{k',\text{T}(k',s),s}$ $(1 \le b \le B)$

**if** $P_{t,b} > P_m$ or $|\mathcal{S}_b| < P$ $(c_f = 0)$ or $|\mathcal{S}_{AP_b}| < P$ $(c_f = 1)$ then

*MC simulation terminates*

**else**

*go to Step 2*

**end if**

**end if**

It should be emphasized at this point that a joint beamforming approach among the active APs is considered. In this case, for each MS in CFA mode, all beamforming configurations of the APs that contribute to PRB allocation are jointly updated, along with the corresponding APs. MS rejection will take place only in the case where there is not any available configuration to serve all active MSs. In the opposite case, all related sets are updated (Step 8) and reject flag ($rf$) is set to zero. MC simulation comes to an end either if power outage occurs in an AP, or if there are no available PRBs for a new potential MS to arrive. In the BSA allocation mode, as previously mentioned, this happens if there are no available PRBs in the $b^{\text{th}}$ BS. In the CFA mode, PRB availability considers the adjacent APs of the candidate MS.

### B. BEAMFORMING PROCEDURES

In this subsection, the proposed beamforming approach will be further explained with the help of Fig. 4. It should be emphasized at this point that the REs per mMIMO configuration gradually increase starting from the activation of the central element (i.e., 1×1 configuration) until the desired QoS is met for all active MSs of the considered AP. To this end, and with respect to Fig. 4, two traffic scenarios have been considered: In the first scenario, MSs are assumed to heavily engage in online streaming activities, which are characterized as bandwidth and energy-hungry applications. To meet this demand, a subarray consisting of 21×3 elements is activated, offering a high gain of 22.8dBi as shown in Fig. 4, ensuring seamless transmission and reception of high-bandwidth content. In contrast, in the second scenario where MSs engage in less bandwidth-intensive texting activities, the requirement for high-quality service is remarkably reduced. Here, a smaller subarray configuration of 3×3 elements will suffice, featuring a lower gain of 14.6dBi, as shown in Fig. 4.
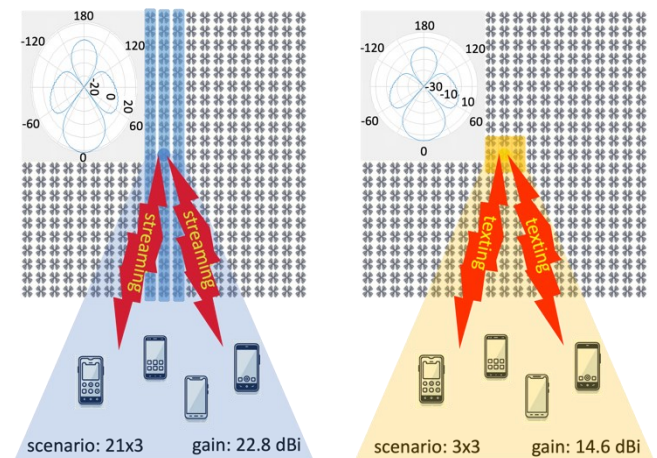


**FIGURE 4. Two propagation scenarios in terms of QoS regarding heavy activity of online streaming and light activity of texting, left and right panel, respectively. The corresponding similar radiation patterns of both scenarios are illustrated on the upper left and right part of each panel.**
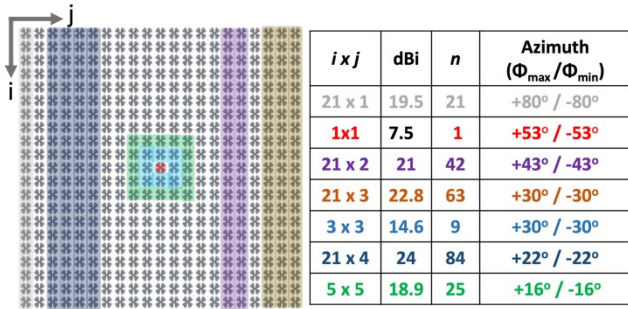
| i x j | dBi | n | Azimuth ($\Phi_{max}/\Phi_{min}$) |
|---|---|---|---|
| 21 x 1 | 19.5 | 21 | +80° / -80° |
| 1x1 | 7.5 | 1 | +53° / -53° |
| 21 x 2 | 21 | 42 | +43° / -43° |
| 21 x 3 | 22.8 | 63 | +30° / -30° |
| 3 x 3 | 14.6 | 9 | +30° / -30° |
| 21 x 4 | 24 | 84 | +22° / -22° |
| 5 x 5 | 18.9 | 25 | +16° / -16° |

**FIGURE 5.** Antenna array geometry with potential activated configurations highlighted in the right panel using corresponding colors. The right panel columns describe the number of activated REs per row and per column, the gain of each array configuration, the total number of REs, and the maximum/minimum azimuth beamwidth of each configuration.

Note that both of the former scenarios require identical spatial coverage as MSs are distributed in the same way. Consequently, both antenna configurations form similar radiation patterns, as shown in Fig.4.

The need for similarity in radiation patterns, as previously highlighted, constitutes one of the most critical parameters of the current work. Specifically, while the radiation patterns exhibit similarity in terms of directivity, there is a significant difference in terms of gain. This is clearly illustrated in Fig. 5, which presents various indicative antenna configurations along with their maximum and minimum obtained azimuth beamwidth and corresponding gain (dBi). Notably, the activation of a single RE can form a beamwidth of 106° with a gain of 7.5 dBi. In contrast, the activation of a 21×2 subarray achieves a comparable beamwidth of 96° but with a substantially higher gain of 21 dBi. Although similar spatial coverage can be achieved with these two different antenna array configurations, the required services will ultimately dictate the most appropriate array scheme.

This adaptive deployment of antenna array underscores the system's ability to tailor resource allocation not only to the specific MS demands but also to the distinct MS locations, thereby optimizing energy efficiency.

## C. PRACTICAL CONSIDERATIONS AND COMPLEXITY CALCULATIONS

In Fig. 6, typical radiation patterns are depicted in the first tier BSs of the central BS (labelled as 1), as in this case CCI is maximized. The red outlines in each pattern indicate the pointing direction of the specific beam. Considering an arbitrary AP in the first BS (i.e., the one corresponding to the pointing direction of the vertical arrow), then the set of adjacent APs takes into consideration only the APs of the neighboring BSs whose radiation patterns might have an impact on CCI (with respect to Fig. 6, these include nine APs that belong to BSs labelled as 2,3,4,5,6 and 7). Therefore, all SINR and SJR calculations consider only a very small subset of the entire APs, that further reduces the computational complexity of the presented calculations.

In realistic CF-mMIMO deployments, if the aforementioned BSs are connected to the same CPU, then latency is minimized for the MSs in the area of the first BS, since all KPI-related calculations (i.e., channel measurements, SINR and SJR, transmit vector matrices, etc.) are executed locally. However, even in the case where adjacent APs belong to different CPUs, virtual clusters can be formulated. For example, with respect to Fig. 1, the virtual cluster for the specific AP of the first BS includes nine adjacent APs, as previously mentioned. The related parameters for each cluster can be locally stored in the corresponding CPUs (i.e., all CPUs that are associated with one or more BSs of the specific cluster) and be updated according to the coherence time of the channel.

Furthermore, by employing cooperative adaptive beamforming, as previously mentioned, that takes into account all APs serving a specific MS and considering the interference (jamming) to other co-channel MSs, the impact of pilot contamination can be minimized. This is also depicted in Fig. 6, since as it becomes apparent there are signals from adjacent APs (i.e., the one from the fifth BS) that are received from the backlobe of the radiation pattern under consideration. As a final remark on this issue, it should be noted that the generated beams in Fig. 6 cover a wide angular space per AP, to depict a worst-case scenario in terms of interference. The effects of cooperative beamforming in the topology are more significant when highly directive beams are generated, since in this case the APs per virtual cluster can be minimized if overlap among beamformers is negligible. Hence, it is important to highlight at this point that the set of adjacent APs for a particular AP of the orientation is not statically defined but is constantly updated according to the radiation patterns of the first tier BSs.

In the worst-case scenario (i.e., CFA mode with dynamic PRB switching) then all $P$ requested PRBs for a new MS that tries to access the network are already assigned to other MSs. In this case, $P$ equivalent PRB switching actions might have to take place. However, as previously mentioned, all related SINR and SJR values for the involved MSs have already been precalculated on MS entrance, based on a small set of adjacent APs. Afterwards, the deployed beamforming configurations in the participating APs might have to change, to ensure QoS in all involved MSs. In this case however, the transition from one state to another involves the activation of additional REs and the formulation of more directional beams. Since a successful transition implies that QoS is met for all PRBs and MSs in the orientation up to this point, in the worst-case scenario all $N_{BC}$ configurations (i.e., 51) would have to be examined. Hence, since each PRB switching affects up to 12 co-channel MSs (i.e., the worst-case scenario involves all 6 first-tier BSs of the considered AP and two PRBs), then the complexity of the proposed approach is proportional to $P \times N_{BC}$.
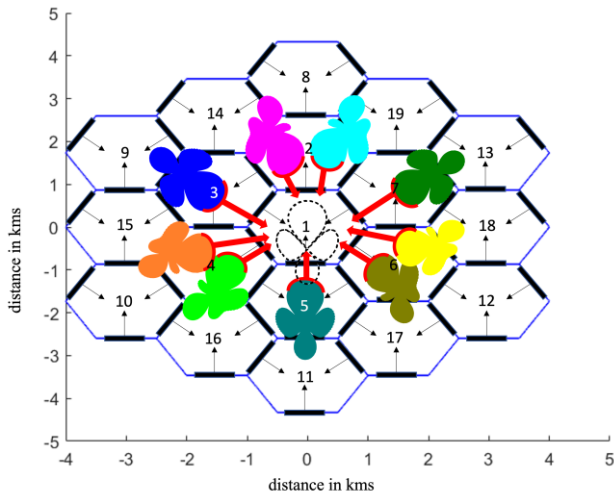
**FIGURE 6.** Radiation patterns in the considered topology (first tier worst case scenario).

## V. PERFORMANCE EVALUATION

Simulations have been carried out with the help of the developed system level simulator that was implemented in Matlab [40] and results are presented in Figs. 8-11. To this end, SE, EE, BP as well as the maximum number of REs in the topology are depicted. The latter term refers to the maximum number of REs per BS and MC simulation. All simulation parameters are summarized in Table I. In this context, 57 APs are considered in a two-tier topology. Moreover, as it is also depicted in Fig. 7, hot spot areas are generated per BS to simulate the performance of the considered orientations in highly demanding traffic scenarios. In this case, an MS can be located inside a hot sport area with probability 1/3 and in the remaining BS area with probability 2/3. In each figure, two PRB allocation approaches are depicted: BSA and CFA, as mentioned in the previous section. To this end, CFA includes static (s) and adaptive (a) PRB assignment. Moreover, two traffic scenarios (TSs) have been considered as well. In the first TS, QPSK modulation per PRB has been assumed. Therefore, considering 15 PRBs per MS, an equivalent requested data rate of 21.6 Mbps is derived. In the second TS, a mixed type of service is now supported, where QPSK/16-QAM/64-QAM modulation per PRB has been considered, for the 50%/30%/20% of the active MSs, respectively.

All output KPIs are presented in the form of cumulative distribution function (CDF) curves. Throughout the rest of this manuscript, all metrics will be compared with respect to their mean values, unless otherwise stated. As it can be observed from Fig. 8, SE in TS1 can reach up to 13.4/10.4/13.4 bps/Hz for the BSA/CFA(s)/CFA(a) PRB allocation modes, respectively. It becomes apparent that SE can deteriorate significantly in the CFA(s) approach, since fewer active MSs are now supported. In this case, the

absence of a dynamic PRB allocation scheme might increase the transmission power of adjacent APs that serve an active MS, which in turn has a direct impact on CCI. Similar conclusions can be drawn for the second traffic scenario (TS2) as well, where corresponding SE values are 22.7/16.1/22.3 bps/Hz, for the BSA/CFA(s)/CFA(a) approaches, respectively. SE deterioration in the CFA(s) case is now more evident, due to the high data rate services that are supported.

In the same context, it follows from Fig. 9 that corresponding values for EE (TS1) are 0.87/0.95/0.99 Mbits/J for the BSA/CFA(s)/CFA(a) approaches, respectively. Hence, an almost 14% gain can be achieved when comparing the CFA and BSA approaches. In TS2, EE values are now 1.63/1.36/1.42 Mbits/J, respectively, for the three aforementioned PRB allocation modes. Therefore, in this case it becomes apparent that EE deteriorates in the CFA(a) scenario, when compared to BSA. However, it is important to note at this point that for a fair comparison among the studied resource allocation considerations (non-CF and CF), the same topology was considered in both scenarios. Therefore, in cases of PRB assignment from adjacent APs, transmission in longer propagation distances would have to be supported with respect to denser network deployments. This becomes more evident for high data rate services, that can reach up to 64.8 Mbps per MS (TS2, Table I). However, in realistic CF orientations, flexible AP deployments and RN transmission can be supported as well, that can significantly enhance system's EE [13].

In Fig. 10, BP is depicted, defined as the ratio of the accepted MSs in the network to the total number of MSs that tried to access the network. In the majority of the considered scenarios, BP is limited to ~1.7%. However, as it can be observed, this metric deteriorates significantly for the CFA(s) PRB allocation mode, for both TSs. In this case, as previously mentioned, since dynamic PRB allocation is not considered, PRB assignment from adjacent APs might have a severe impact on CCI, which in turn results in increased MS rejection probability.

Finally, in Fig. 11, the total number of REs in the topology is depicted, for all the considered PRB allocation modes. In this case, active REs are 618/470/601 for the BSA/CFA(s)/CFA(a) allocation approaches, respectively (TS1). As it can be observed, active REs are reduced in the CFA(a) approach, when compared to BSA. Although there is a further reduction in the CFA(s) approach, this is accompanied by increased BP and reduced SE, as previously mentioned. Similar conclusions can be drawn for TS2 as well, where active REs are now 854/518/705 for the aforementioned allocation approaches, respectively (BSA/CFA(s)/CFA(a)). Hence, as it becomes apparent, the reduction percentage of REs among the CFA(a) and BSA approaches is now more evident compared to TS1.
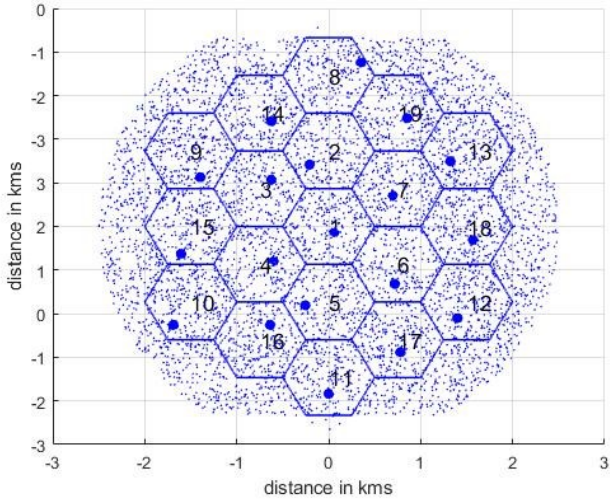
FIGURE 7. Multicellular orientation with non-uniform traffic.



FIGURE 8. Spectral efficiency (bps/Hz).

TABLE I
SIMULATION PARAMETERS

| Parameter | Value or Assumption |
|---|---|
| Number of cells | 19 |
| Access points per cell | 3 |
| Cell radius ($m$) | 500 [41] |
| Total bandwidth (MHz) | 100 |
| Pathloss model | UMa |
| Std for shadow fading (dB) | 6 |
| Carrier frequency (GHz) | 28 |
| Subcarrier spacing (kHz) | 60 |
| Subcarriers per PRB | 12 |
| PRBs per BS ($N_{PRB}$) | 132 |
| Number of clusters ($N$)/Subpaths per cluster ($M$) | 6/20 |
| Requested PRBs per MS | 15 |
| Monte Carlo snapshots per scenario | $10^3$ |
| Antenna elements per MS ($N_r$) | 2 |
| Beamforming configurations ($N_{BC}$) | 51 |
| Maximum transmission power per BS/MS ($P_m/p_m$) (W) | 20/1 |
| Required $E_b/N_o$ (dB) for QPSK/16-QAM/64-QAM modulation ($SNR_{th}$) | 9.6/16.4/22.7 [42] |
| Transmission rate per MS for QPSK/16-QAM/64-QAM modulation (Mbps) | 21.6/43.2/64.8 |

It is interesting to note from the analysis of the four considered KPIs, that the proposed CFA(a) approach can improve various performance metrics in TS1, such as EE and number of REs. In TS2, although EE deteriorates with respect to BSA, as previously mentioned, the reduced number of active REs (almost 17%), has a direct impact on the hardware complexity and computational burden reduction. In this case, beamforming calculations are performed on a reduced subset of REs. Hence, the deployment of the CFA(a) approach can be quite promising in dense CF-mMIMO orientations with flexible AP positioning. All KPIs with respect to their mean values are also summarized in Table II.
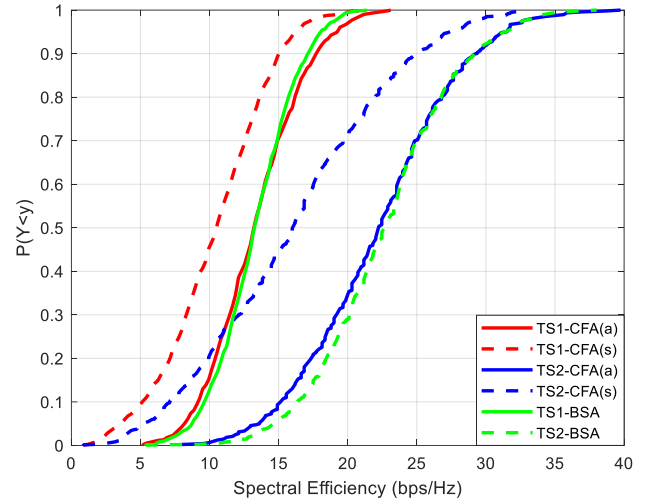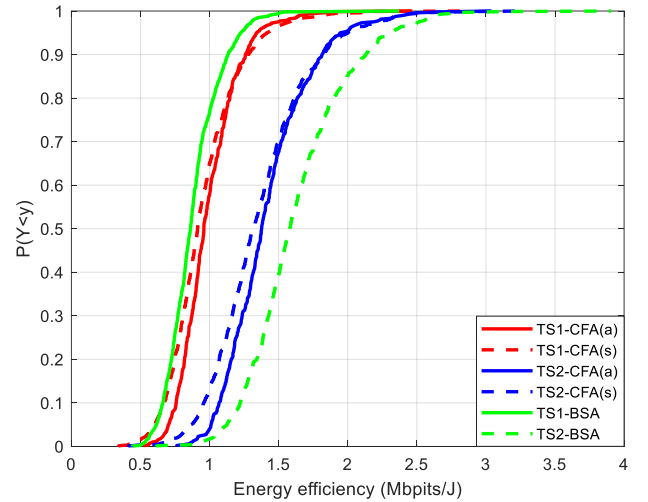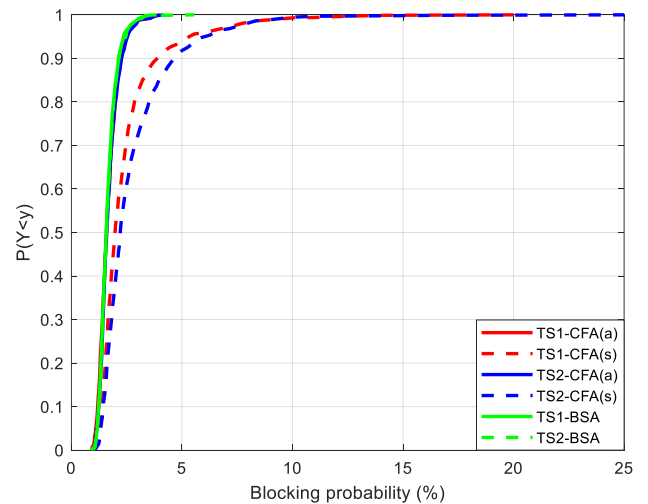


FIGURE 9. Energy efficiency (Mbits/J).



FIGURE 10. Blocking probability.

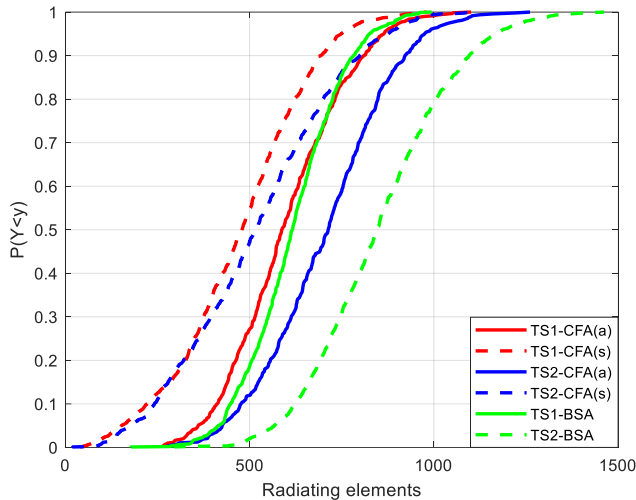**FIGURE 11.** Number of radiating elements in the topology.

TABLE II
KPI COMPARISON IN TERMS OF MEAN VALUES

| Parameter | TS 1 | | | TS 2 | | |
|---|---|---|---|---|---|---|
| | BSA | CFA(s) | CFA(a) | BSA | CFA(s) | CFA(a) |
| SE (bps/Hz) | 13.4 | 10.4 | 13.4 | 22.7 | 16.1 | 22.3 |
| EE (Mbits/J) | 0.87 | 0.95 | 0.99 | 1.63 | 1.36 | 1.42 |
| BP (%) | 1.66 | 2.49 | 1.68 | 1.67 | 2.80 | 1.71 |
| REs | 618 | 470 | 601 | 854 | 518 | 705 |

## VI. CONCLUSIONS

The performance of cell-free massive MIMO configurations in multicellular setups has been assessed using a specially developed system-level simulator, and its results were benchmarked against traditional centralized resource allocation scenarios. Within this framework, a dynamic physical resource block allocation method was introduced and evaluated. According to the presented results, energy efficiency in the cell-free massive MIMO orientation can be improved up to 14% compared to the conventional centralized transmission approach. Although this gain deteriorates for high data rate services, the equivalent reduction on the number of radiating elements, which is associated with reduced hardware and computational burden, indicates promising results in denser network deployments with dynamic access point positioning.

Future work, among others, includes the optimum placement of access points and relay nodes in the topology, as well as the deployment of machine learning approaches that can provide more flexible decisions on the association of mobile users with specific access points.

## REFERENCES

[1] P. Popovski, K. F. Trillingsgaard, O. Simeone, and G. Durisi, "5G wireless network slicing for eMBB, URLLC, and mMTC: A communication-theoretic View," *IEEE Access*, vol. 6, pp. 55765-55779, 2018, doi: 10.1109/ACCESS.2018.2872781.

[2] S. Gallenmüller, J. Naab, I. Adam, and G. Carle, "5G URLLC: A case study on low-latency intrusion prevention," *IEEE Commun. Mag.*, vol. 58, no. 10, pp. 35-41, Oct. 2020, doi: 10.1109/MCOM.001.2000467.

[3] C. Bockelmann et al., "Towards massive connectivity support for scalable mMTC communications in 5G networks," *IEEE Access*, vol. 6, pp. 28969-28992, 2018, doi: 10.1109/ACCESS.2018.2837382.

[4] A. N. Uwaechia, and N. M. Mahyuddin, "A comprehensive survey on millimeter wave communications for fifth-generation wireless networks: Feasibility and challenges," *IEEE Access*, vol. 8, pp. 62367-62414, 2020, doi: 10.1109/ACCESS.2020.2984204.

[5] E. G. Larsson, O. Edfors, F. Tufvesson, and T. L. Marzetta, "Massive MIMO for next generation wireless systems," *IEEE Commun. Mag.*, vol. 52, no. 2, pp. 186-195, Feb. 2014, doi: 10.1109/MCOM.2014.6736761.

[6] B. Makki, K. Chitti, A. Behravan, and M.-S. Alouini, "A survey of NOMA: Current status and open research challenges," *IEEE Open J. Commun*. Soc., vol. 1, pp. 179-189, 2020, doi: 10.1109/OJCOMS.2020.2969899.

[7] Z. Wang, Y. Liu, X. Mu, Z. Ding, and O. A. Dobre, "NOMA empowered integrated sensing and communication", *IEEE Commun. Lett.*, vol. 26, no. 3, pp. 677-681, March 2022, doi: 10.1109/LCOMM.2022.3140271.

[8] Z. Wang, X. Mu, and Y. Liu, "Near-field integrated sensing and communications," *IEEE Commun. Lett.*, vol. 27, no. 8, pp. 2048-2052, Aug. 2023, doi: 10.1109/LCOMM.2023.3280132.

[9] A. Bazzi, and M. Chafii, "On integrated sensing and communication waveforms with tunable PAPR," *IEEE Trans. Wirel. Commun.*, vol. 22, no. 11, pp. 7345-7360, Nov. 2023, doi: 10.1109/TWC.2023.3250263.

[10] J. Erfanian, D. Lister, Q. Zhao, G. Wikström, and Y. Chen, "6G vision & analysis of potential use cases," *IEEE Commun. Mag.*, vol. 61, no. 4, pp. 12-14, April 2023, doi: 10.1109/MCOM.2023.10106181.

[11] L. U. Khan, I. Yaqoob, M. Imran, Z. Han, and C. S. Hong, "6G wireless systems: A vision, architectural elements, and future directions," *IEEE Access*, vol. 8, pp. 147029-147044, 2020, doi: 10.1109/ACCESS.2020.3015289.

[12] S. Andreev, V. Petrov, M. Dohler, and H. Yanikomeroglu, "Future of ultra-dense networks beyond 5G: Harnessing heterogeneous moving cells," *IEEE Commun. Mag.*, vol. 57, no. 6, pp. 86-92, Jun. 2019, doi: 10.1109/MCOM.2019.1800056.

[13] I. A. Bartsiokas, P. K. Gkonis, D. I. Kaklamani, and I. S. Venieris, "A DL-enabled relay node placement and selection framework in multicellular networks," *IEEE Access*, vol. 11, pp. 65153-65169, 2023, doi: 10.1109/ACCESS.2023.3290482.

[14] S. Elhoushy, M. Ibrahim, and W. Hamouda, "Cell-Free massive MIMO: A Survey," *IEEE Commun. Surv. Tutor.*, vol. 24, no. 1, pp. 492-523, Firstquarter 2022, doi: 10.1109/COMST.2021.3123267.

[15] H. Q. Ngo, A. Ashikhmin, H. Yang, E. G. Larsson, and T. L. Marzetta, "Cell-free massive MIMO versus small cells," *IEEE Trans. Wirel. Commun.*, vol. 16, no. 3, pp. 1834-1850, March 2017, doi: 10.1109/TWC.2017.2655515.

[16] E. Björnson, and L. Sanguinetti, "Scalable cell-free massive MIMO systems," *IEEE Trans. Commun.*, vol.

68, no. 7, pp. 4247-4261, Jul. 2020, doi: 10.1109/TCOMM.2020.2987311.

[17] P. K. Gkonis, "A survey on machine learning techniques for massive MIMO configurations: Application areas, performance limitations and future challenges," *IEEE Access*, vol. 11, pp. 67-88, 2023, doi: 10.1109/ACCESS.2022.3232855.

[18] X.-T. Dang, H. V. Nguyen, and O.-S. Shin, "Optimization of IRS-NOMA-assisted cell-free massive MIMO systems using deep reinforcement learning," *IEEE Access*, vol. 11, pp. 94402-94414, 2023, doi: 10.1109/ACCESS.2023.3310283.

[19] H. A. Ammar, R. Adve, S. Shahbazpanahi, G. Boudreau and K. V. Srinivas, "User-centric cell-free massive MIMO networks: A survey of opportunities, challenges and solutions," *IEEE Commun. Surv.*, vol. 24, no. 1, pp. 611-652, Firstquarter 2022, doi: 10.1109/COMST.2021.3135119.

[20] D. Löschenbrand, M. Hofer, L. Bernadó, S. Zelenbaba, and T. Zemen, "Towards cell-free massive MIMO: A measurement-based analysis," *IEEE Access*, vol. 10, pp. 89232-89247, 2022, doi: 10.1109/ACCESS.2022.3200365.

[21] U. Demirhan, and A. Alkhateeb, "Enabling cell-free massive MIMO systems with wireless millimeter wave fronthaul," *IEEE Trans. Wirel. Commun.*, vol. 21, no. 11, pp. 9482-9496, Nov. 2022, doi: 10.1109/TWC.2022.3177186.

[22] H. Zhang, R. Su, Y. Zhu, K. Long, and G. K. Karagiannidis, "User-centric cell-free massive MIMO system for indoor industrial networks," *IEEE Trans. Commun.*, vol. 70, no. 11, pp. 7644-7655, Nov. 2022, doi: 10.1109/TCOMM.2022.3210410.

[23] A. L. P. Fernandes, D. D. Souza, D. B. da Costa, A. M. Cavalcante, and J. C. W. A. Costa, "Cell-free massive MIMO with segmented fronthaul: Reliability and protection aspects," *IEEE Wirel. Commun.*, vol. 11, no. 8, pp. 1580-1584, Aug. 2022, doi: 10.1109/LWC.2022.3166485.

[24] J. Zheng, J. Zhang, J. Cheng, V. C. M. Leung, D. W. K. Ng, and B. Ai, "Asynchronous cell-free massive MIMO with rate-splitting," *IEEE J. Sel. Areas Commun.*, vol. 41, no. 5, pp. 1366-1382, May 2023, doi: 10.1109/JSAC.2023.3240709.

[25] Ö. T. Demir, M. Masoudi, E. Björnson, and C. Cavdar, "Cell-free massive MIMO in virtualized CRAN: How to minimize the total network power?," *ICC 2022 - IEEE International Conference on Communications, Seoul, Korea, Republic of*, 2022, pp. 159-164, doi: 10.1109/ICC45855.2022.9838846.

[26] Q. Peng, H. Ren, C. Pan, N. Liu, and M. Elkashlan, "Resource allocation for cell-free massive MIMO enabled URLLC downlink systems," *2022 IEEE/CIC International Conference on Communications in China (ICCC)*, Sanshui, Foshan, China, 2022, pp. 838-843, doi: 10.1109/ICCC55456.2022.9880834.

[27] S. Kamiwatari, I. Kanno, T. Hayashi, and Y. Amano, "RF chain-wise clustering schemes for millimeter wave cell-free massive MIMO with centralized hybrid beamforming," *IEEE Access*, vol. 12, pp. 19682-19693, 2024, doi: 10.1109/ACCESS.2024.3360716.

[28] Y. Xiong et al., "Data-aided channel estimation and combining for cell-free massive MIMO with low-resolution ADCs," *IEEE Commun. Lett.*, doi: 10.1109/LCOMM.2024.3357214.

[29] M. Ito, S. Fukue, K. Ando, I. Kanno, K. Yamazaki, and K. Ishibashi, "Clustering and beamforming for user-centric cell-free massive MIMO with backhaul capacity limitation," *IEEE Access*, vol. 12, pp. 382-395, 2024, doi: 10.1109/ACCESS.2023.3346903.

[30] H. Zhao, Y. Zhang, W. Xia, Y. Ni, L. Yang, and H. Zhu, "Distributed opportunistic power control for uplink cell-

free massive MIMO-IoT networks under ricean fading channels," *IEEE Trans. Netw. Service Manag*, doi: 10.1109/TNSM.2023.3342909.

[31] X. Qiao, Y. Zhang, H. Zhao, L. Yang, and H. Zhu, "Two-layer large scale fading precoding for cell-free massive MIMO: Performance analysis and optimization," *IEEE Trans. Veh. Technol.*, doi: 10.1109/TVT.2023.3327745.

[32] Q. Sun et al., "Uplink performance of hardware-impaired cell-free massive MIMO with multi-antenna users and superimposed pilots," *IEEE Trans. Commun.*, vol. 71, no. 11, pp. 6711-6726, Nov. 2023, doi: 10.1109/TCOMM.2023.3301071.

[33] *Study Channel Model for Frequencies From 0.5 to 100 GHz*, document TR 38.901, 3GPP, Version 14.3.0, Release 14, 2018.

[34] *5G NR Physical Channels and Modulation*, document TS 138 211, 3GPP, Version 15.3.0, Release 15, 2018.

[35] S. Qu, and C. Ruan, "Effect of round corners on bowtie antennas," *Prog. Electromagn. Res.*, vol. 57, pp. 179-195, 2006, doi:10.2528/PIER05072103.

[36] W. C. Zheng, L. Zhang, Q. X. Li, and Y.Leng, "Dual-band dual-polarized compact bowtie antenna array for anti-interference MIMO WLAN," *IEEE Trans. Antennas Propag.*, vol. 62, no. 1, pp. 237–246, 2014, doi: 10.1109/TAP.2013.2287287.

[37] S. Lavdas, P. K. Gkonis, Z. Zinonos, P. Trakadas, L. Sarakis, and K. Papadopoulos, "A machine learning adaptive beamforming framework for 5G millimeter wave massive MIMO multicellular networks," *IEEE Access*, vol. 10, pp. 91597-91609, 2022, doi: 10.1109/ACCESS.2022.3202640.

[38] S. Lavdas, P. K. Gkonis, E. Tsaknaki, L. Sarakis, P. Trakadas, and K. Papadopoulos, "A deep learning framework for adaptive beamforming in massive MIMO millimeter wave 5G multicellular networks," *Electronics*, vol. 12, no. 17, 2023, https://doi.org/10.3390/electronics12173555.

[39] C. Balanis, *Antenna Theory: Analysis and Design*. Hoboken, NJ, USA: Wiley, 2026.

[40] MATLAB, version 9.11.0 (R2021b). Natick, Massachusetts: The MathWorks Inc., 2021.

[41] A. Giannopoulos, S. Spantideas, N. Kapsalis, P. Karkazis, and P. Trakadas, "Deep reinforcement learning for energy-efficient multi-channel transmissions in 5G cognitive HetNets: Centralized, decentralized and transfer learning based solutions," *IEEE Access*, vol. 9, pp. 129358-129374, 2021, 10.1109/ACCESS.2021.3113501.

[42] R. Giuliano, C. Monti, and P. Loreti, "WiMAX fractional frequency reuse for rural environments," *IEEE Wireless Commun.*, vol. 15, no. 3, pp. 60–65, Jun. 2008, doi: 10.1109/MWC.2008.4547524.

**PANAGIOTIS K. GKONIS** is an Assistant Professor at the Department of Digital Industry Technologies of the National and Kapodistrian University of Athens (NKUA). He received the Diploma Degree in Electrical and Computer Engineering and PhD degree from the Electrical and Computer Engineering School of National Technical University of Athens (NTUA), Greece, in 2005 and 2009, respectively. He has also received the MSc in Engineering-Economic Systems Programme from NTUA, in 2009. From 2010 to 2015 he worked as a postdoctoral researcher in the Intelligent Communications and Broadband Networks Laboratory (ICBNET) of NTUA. Moreover, he has also served as Scientific/Laboratory Associate of the former Technological Institute of Sterea Ellada, in the Departments of Electrical and Aircraft Engineering, respectively. He is an author/co-author of more than seventy (70) scientific publications in international journals, scientific conferences and book chapters, in the areas of wireless networks, broadband communications as well as computational modelling of cellular networks. As a researcher, he has participated in various national and European funded projects.

**SPYROS LAVDAS** graduated from the Faculty of Engineering of Democritus University of Thrace (DUTH), Xanthi, Greece – Electrical & Computer Engineer in 2009. He also took his Master Diploma in Computational Electromagnetics in the department of computer systems and satellite telecommunications of DUTH in 2012 and he was awarded his Ph.D. in Silicon Photonics from the department of Electronic and Electrical Engineering of University College London (UCL) in 2015. He has participated in European research programs (V-smmart nano, FP7) and he has also worked in the RnD department of Integrated System Development company in Athens. He has academic experience of teaching undergraduate and post graduate students the courses of Microwaves, Optical Nonlinearities and Problem-Solving Methods. Spyros is currently teaching Problem Solving Methods in Neapolis University Pafos. He is also an instructor in the American College of Greece. His main research interests are focused in the area of computational electromagnetics, silicon photonics, nano-antennas, 5G and 6G communications.

**GEORGIOS VARDOULIAS** received the Diploma degree in Electrical and Computer Engineering from the National Technical University of Athens, in 1997, and the Ph.D. degree from the University of Edinburgh, Edinburgh, U.K., 2001. He is currently an Assistant Professor at The American College of Greece and a Senior Research Engineer at Intracom Defense. Previous positions include Motorola U.K., the Hellenic Naval Academy and the National Centre of Scientific Research "Demokritos". He has participated as a researcher and a project manager in numerous industrial and EU-funded research and development projects. His research interests include coexistence of Software Defined Radio and Software Defined

Networking technologies in tactical wireless networks, Federated Learning systems for the defense sector, and the application of advanced Digital Signal Processing and machine learning techniques in predictive maintenance for naval rotating equipment.

**PANAGIOTIS TRAKADAS** received his Dipl-Ing. Degree in Electrical & Computer Engineering and his Ph.D. from the National Technical University of Athens (NTUA). Currently, he is an Associate Professor at National and Kapodistrian University of Athens. His research interests are in the fields of wireless and mobile communications, wireless sensor networking, network function virtualization and cloud computing. He has published more than 130 papers in magazines, journals, and conference proceedings. In the past, he was working for Hellenic Aerospace Industry (HAI), as a Senior Engineer, on the design of military wireless telecommunications systems and he was also working for the Hellenic Authority for Communications Security and Privacy, where he was holding the position of Director of the Division for the Assurance of Infrastructures and Telecommunications Services Privacy. He is a reviewer in several journals including IEEE Transactions on Communications and IEEE Transactions on Electromagnetic Compatibility journals. Dr. Trakadas has been actively involved in many EU FP7 and H2020 research projects.

**LAMBROS SARAKIS** (Member, IEEE) received the Diploma degree in electrical and computer engineering from the National Technical University of Athens (NTUA), in 1996, the M.Sc. degree in communications and signal processing from Imperial College London, in 1997, and the Ph.D. degree in computer engineering from NTUA, in 2002. From 2004 to 2010, he served as an Assistant Researcher for the Institute of Informatics and Telecommunications, National Centre for Scientific Research "Demokritos", Greece. He is currently an Associate Professor with the Department of Digital Industry Technologies, National and Kapodistrian University of Athens. He has participated in several research projects at national and international scale in research and management capacities. His research interests include 5G networks, sensor, mobile ad-hoc and opportunistic vehicular networks, communication systems for smart grids, mobility management in heterogeneous wireless networks, and hardware/software codesign for embedded systems. He has more than 60 publications in books, and journals and conference proceedings in the above areas. He has served on the technical program or organizing committee for several conferences and workshops.

**IEEE** *Access*
Multidisciplinary : Rapid Review : Open Access Journal

**KONSTANTINOS PAPADOPOULOS** graduated from the department of Electrical Engineering, National Technical University of Athens in 1990 and he received his PhD degree from the same department in 1996. From 1997 to 2002 he worked as a consultant for various Greek firms. From 2002 to 2004 he worked for the General Secretariat of Industry of the Greek Ministry of Development. From 2004 to 2021 he served as Associate Professor and Professor in departments of Higher education. Since 2021 he serves as a Professor in the Department of Digital Industry Technologies of the National and Kapodistrian University of Athens. Since 2014 he participates in the steering committee of the postgraduate program entitled "Intelligent management of Renewable Energy Systems". He also participates in teaching of the modules "Production and Storage of Energy" and "Electricity markets and Standards". His published papers have been cited more than 400 times by other researchers (h-index 11, scopus). His research interests include microelectronics, sensors and smart grids.